DIASTOLIC PRESSURE-VOLUME RELATIONS AND DISTRIBUTION OF PRESSURE AND FIBER EXTENSION ACROSS THE WALL OF A MODEL LEFT VENTRICLE

THEODORE S. FEIT, *Department of Nuclear Medicine, San Francisco Veterans Administration Hospital, San Francisco, California 94121 U.S.A.*

ABSTRACT A model for left ventricular diastolic mechanics is formulated that takes into account noneligible wall thickness, incompressibility, finite deformation, nonlinear elastic effects, and the known fiber architecture of the ventricular wall. The model consists of a hollow cylindrical mass of muscle bound between two plates of negligible mass. The wall contains fiber elements that follow a helical course and carry only axial tension. The fiber angle (i.e., helical pitch) is constant along the length of each fiber but varies through the wall in accordance with the known distribution of fiber orientations in the canine left ventricle. To simplify the analysis and reduce the number of degrees of freedom, the anatomic distribution of fiber orientations is divided into a clockwise and counterclockwise system. The reference configuration for the model corresponds to a state in which, by hypothesis, the transmural pressure gradient is zero, the tension is zero for all fibers across the wall, and all fibers are assumed to have a sarcomere length of 1.9 μm. This choice of reference configuration is based on the empirical evidence that canine ventricles, fixed in a state of zero transmural pressure gradient and dissected, demonstrate sarcomere lengths between 1.9 and 2.0 μm in inner, middle, and outer wall layers, while isolated ventricular muscle bundles are observed to have zero resting tension when the sarcomere length ranges from 1.9 to 2.0 μm. An equation representing the global condition for equilibrium is derived and solved numerically. It is found that the model's pressure-volume relation is representative of diastolic filling in vivo over a wide range of filling pressures, and the calculated midwall sarcomere lengths in the model compare favorably with published experimental data. Subendocardial fibers are stretched beyong L_{max} even at low filling pressures, i.e., 5 mm Hg, while fibers located between 60–80% of wall thickness extend minimally between 5 and 12 mm Hg. The hydrostatic pressure field within the wall is highly nonlinear. The pressure rises steeply in the subendocardial layers so that the net gain in pressure in the inner third of the wall is 85% of the filling pressure. It is demonstrated that these results are independent of heart size for a family of heart models that are scale models of each other. They are, however, critically dependent on the existence of longitudinally oriented fibers in the endocardial and epicardial regions of heart wall.

INTRODUCTION

A precise knowledge of diastolic ventricular mechanics is essential for understanding the behavior of the heart in normal and pathological states. A realistic model of the diastolic left ventricle should take into account the known anatomic structure of the ventricular wall and the key mechanical properties of its muscle fibers.

Dr. Feit's present address is Department of Nuclear Medicine, St. Joseph Medical Center, Burbank, Calif. 91505.

The ventricular wall is composed of ordered sets of interconnected muscle fibers, with each set characterized by a predominant fiber direction. The muscle fibers follow a helical course in the wall, with the fiber angle (i.e., helical pitch) changing smoothly across the wall (Streeter, 1969; Streeter et al., 1969, 1978). Near the inner and outer walls, the course of the fibers is predominantly longitudinal, while in the midwall the fibers are predominantly circumferential. Diastolic filling is thought to alter the degree of extension of the extremely length-sensitive muscle fibers within the walls of the heart, thereby accounting for Starling's Law of the Heart (Patterson and Starling, 1914).

Isolated muscle experiments have established the basic mechanical features of cardiac muscle that need to be incorporated into any realistic formulation of diastolic ventricular mechanics. The resting tension of cardiac muscle is a nonlinear exponential function of its finite degree of extension in the fiber direction (Braunwald et al., 1976). As the resting muscle is passively shortened to ~85% of L_{max} it becomes slack, i.e., the resting tension becomes zero (Braunwald et al., 1976). The developed tension drops precipitously in this same length-range to ~40% of its peak value (Braunwald et al., 1976). L_{max} represents here the fiber length at which active tension is maximal.

In this paper we formulate a mathematical model of the end diastolic left ventricle that allows one to take into account the features of cardiac anatomy and physiology outlined above. The model consists of a thick-walled, hollow, cylindrical mass of muscle bound between two plates of negligible mass. The wall contains fiber elements that follow a helical course and carry only axial tension. The forces exerted by the fiber elements are not known in advance. Instead, wall forces and the geometric configuration of the heart muscle are interdependent. An equation that determines the possible end diastolic configurations of the heart model is derived and solved numerically.

The model used in this paper to analyze diastolic ventricular mechanics differs significantly from previous model work on the diastolic left ventricle. One of two general approaches has been taken in the past: the first considers the myocardium to be a thick-walled solid of revolution having isotropic elastic properties (Janz and Grimm, 1973; Janz et al., 1974; Janz and Waldron, 1978; Mirsky, 1969; Mirsky et al., 1974), while the second approach takes into account local fiber geometry but assumes that the fiber force is constant across the wall and ignores the global constraints imposed by diastolic filling (Streeter, 1969; Streeter et al., 1970). Our results suggest that neither of these approaches can provide a realistic representation of the heart wall in diastole.

Formulations of Equations

Representing the heart in terms of a model presents a problem, for any model of the heart is an idealization and is a woeful imitation of nature. The more closely the complicated details of cardiac anatomy are embodied in a model, the more unmanageable it becomes from a mathematical point of view. Thus, we need to invent a model that retains the significant features of cardiac anatomy and physiology, but in a simplified form, so that the properties of a model can be handled mathematically and studied conveniently. The features that should be taken into account in the formulation of a realistic model of the end diastolic left ventricle include the nonnegligible wall thickness, incompressibility, finite deformation, nonlinear elastic effects, the known fiber architecture of the ventricular wall, and the fact that the heart accommodates volume both by circumferential and longitudinal expansion.

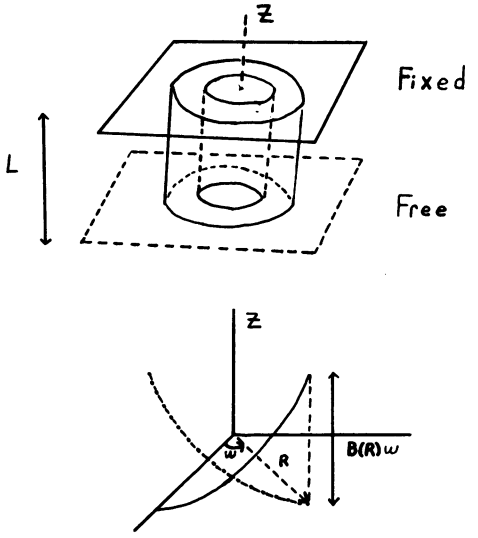

FIGURE 1

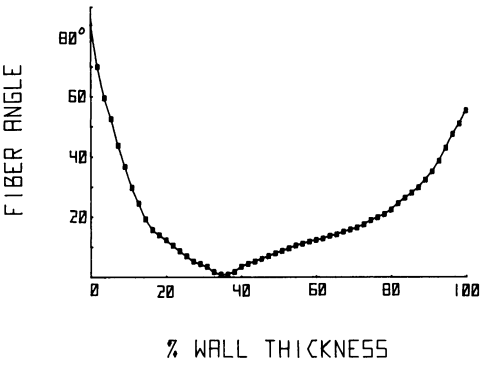

FIGURE 2

FIGURE 1 (top) Schematic diagram of the model left ventricle in the reference configuration. The axial length is L; the inner radius is R_i; the outer radius is R_o. The volume of the inner chamber is $\overline{V} = \pi R_i^2 L$. The model accommodates increases in volume by axial and circumferential expansion. The ends of the cylinder slide tangentially to the plates, so that the model retains its cylindrical configuration. (bottom) The curvilinear solid (——) and dotted (------) lines illustrate the course in space of two muscle fibers in the model wall in the reference configuration. These two fibers are representative of the two fiber systems. The fibers remain a distance R from the central axis of the cylinder. For each angular displacement ω, the Z coordinate of a fiber changes by $B(R)|\omega|$. As R varies between R_i and R_o, B changes smoothly.

FIGURE 2 The distribution of fiber angles across the wall of the heart model. By convention, 0% of wall thickness corresponds to the inner surface; 100% wall thickness corresponds to the outer surface.

With these considerations in mind, we represent the left ventricle in end diastole as a thick-walled, hollow, cylindrical mass of muscle bound between two plates of negligible mass. One plate is fixed in space and corresponds to the base of the heart. To avoid end effects, we assume that the muscle can slide freely tangentially to the plates to retain its cylindrical geometry. The thick walls of this heart model contain fiber elements that follow a helical course. The model and its associated fiber geometry are illustrated in Fig. 1. The radial distance of a fiber from the axis of the cylinder and the fiber angle (i.e., helical pitch) remain constant along the length of each fiber. However, the fiber angle varies through the wall.

Considerable simplification of a model of the heart in diastole can be effected if the model accommodates increases in chamber volume without undergoing twisting. Studies of the left ventricle in diastole utilizing biplane cinefluorography provide empirical evidence that the mammalian heart does not in fact twist significantly during diastolic filling. Nobel et al., (1969) inserted multiple tantalum screws into the left ventricular endocardium of dogs until the cavity was completely outlined in both the anteroposterior and lateral projections. After the dogs recovered from this procedure, the motion of the screws during diastole was studied in vivo by biplane cineradiography. Symmetrical outward movement of the tantalum markers was observed throughout diastole in all cases. The radiologically determined outlines of the ventricular cavity in the anteroposterior and lateral projections were used to numerically

calculate the ventricular volume. When a postmortem heart previously labeled with tantalum screws was passively filled with known amounts of saline, the known changes in volume compared favorably with the changes in volume calculated from the x-ray data describing the positions of the screws in two orthogonal projections. If the ventricle twisted as it filled, one would not expect the x-ray method to be accurate.

The evidence cited above suggests that it is reasonable to devise a diastolic heart model in which twisting motion is avoided. To accomplish this and at the same time retain variable fiber angle across the wall as a feature of the model, we divide the fibers into two systems. For one system, the fiber angle varies between approximately $+80°$ on the inside to $-60°$ on the outside, in a manner similar to that which exists in the ventricular wall (Streeter et al., 1969, 1978). For the second system, the fiber angle varies between approximately $-80°$ on the inside to $+60°$ on the outside, with the fiber angle equal in magnitude and opposite in sign to the first system. The distribution of the absolute value of fiber angles across the wall of the heart model for the two fiber systems is illustrated in Fig. 2. Since the fibers in the two systems follow the same helical course but have opposite sense, the heart model accomodates changes in chamber volume by circumferential expansion and axial extension, similar to the observed motion of the left ventricle during diastolic filling. The cylindrical configuration of the model is maintained at all times.

To represent this heart model mathematically, we select one particular configuration and refer everything concerning the heart to the configuration. In the following mathematical development the choice of reference configuration is arbitrary. In actuality, for any model of left ventricular diastolic mechanics, the choice of the reference configuration is itself a crucial aspect of the model and should be based on physiological considerations and the known material properties of heart muscle. We proceed here with a general formulation of equations and defer discussion of the particular reference configuration to be adopted until the following section.

It is convenient to use cylindrical coordinates. Let $(R, \hat{\theta}, Z)$ represent the position of a material point M in the reference configuration. The $Z = 0$ plane corresponds to the fixed top plate of the heart, while the $Z = L$ plane corresponds to the free plate. Suppose that a fiber intersects the $Z = 0$ plane at the point $(R, \hat{\theta}_0, 0)$. The equations describing the helical path of this fiber in space can be written in the form

$$\text{and } R = R_0, \tag{1a}$$

$$\hat{\theta} = \hat{\theta}_0 + \omega, \tag{1b}$$

$$\text{and } Z = B(R)\omega, \tag{1c}$$

where ω represents the angular displacement and is the independent parameter. $B(R)$ has dimensions of length and is related to the helical fiber angle γ by the relation

$$\frac{B(R)}{R} = \tan \gamma. \tag{2}$$

We now want to examine how the position of the point M at an arbitrary end diastolic configuration (r, θ, z) relates to its position $(R, \hat{\theta}, Z)$ in the reference configuration. By symmetry $\hat{\theta} = \theta$. If point M is located on the free planar edge of the heart, $Z = L$ and $z = L'$,

where L and L' are the respective heart lengths. On the other hand, when M is located on the fixed end of the heart $Z = 0$ and $z = 0$. The coordinate z must vary linearly between these extremes. Therefore

$$z = \lambda Z, \text{ where } \lambda = \frac{L'}{L}. \tag{3}$$

The dimensionless parameter λ represents the axial extension of the heart model, relative to the reference configuration.

Since heart muscle is known to be incompressible, the volume of every part of the heart wall must not change as the wall deforms. Local incompressibility thus requires

$$r\,dr\,d\theta\lambda\,dZ = R\,dR\,d\theta\,dZ. \tag{4}$$

Integrating Eq. 4 we have

$$r^2 = \frac{1}{\lambda}(R^2 + C). \tag{5}$$

Let R_i stand for the inner radius of the heart wall in the reference configuration; r_i is the corresponding radius in an arbitrary end diastolic configuration.

Then

$$\pi r_i^2 \lambda L = \pi R_i^2 L + C\pi L, \tag{6a}$$

so that the constant of integration C is

$$C = \frac{V - \overline{V}}{\pi L}, \tag{6b}$$

where V is the chamber volume in the arbitrary configuration and $\overline{V}$ is the chamber volume in the reference configuration.

The position of point M in 3-space in an arbitrary configuration is

$$\left\{\left[\frac{1}{\lambda}\left(R^2 + \frac{V - \overline{V}}{\pi L}\right)\right]^{1/2}, \theta, \lambda Z\right\}.$$

The configuration of the heart model is determined by the parameters λ and V.

Let T be the net force acting across a muscle fiber. Let $\underset{\sim}{\tau}$ be a unit vector pointing along the fiber in the reference configuration. Let $\underset{\sim}{t}$ be a unit vector pointing along the fiber in a possible end diastolic configuration.

Consider an area element $\underset{\sim}{d}A$ in the reference configuration that maps into an area element $\underset{\sim}{d}a$ in a possible end diastolic configuration. Now a fiber that cuts across $\underset{\sim}{d}A$ will also cut acorss $\underset{\sim}{d}a$, so that the number of fibers dN that cut across the area element does not change. Let $\underset{\sim}{d}F$ represent the total fiber force due to one system of fibers acting across $\underset{\sim}{d}a$ in a possible end diastolic configuration. Then

$$\underset{\sim}{d}F = \tfrac{1}{2}\rho(\underset{\sim}{n} \cdot \underset{\sim}{\tau})T\,dA\underset{\sim}{t} = dNT\underset{\sim}{t}, \tag{7}$$

where $\frac{1}{2}\rho$ = number of fibers in one system per unit cross-sectional area normal to the fiber

direction in the reference configuration, and $\underset{\sim}{n}$ = unit vector perpendicular to the area element dA in the reference configuration. The factor ½ has to be included because we have split the total number of fibers into two systems.

Let $\underset{\sim}{i}_r$, $\underset{\sim}{i}_\theta$, and $\underset{\sim}{i}_z$ be a set of unit vectors that point along the coordinate lines. Let $\underset{\sim}{d}F_\theta$ be the "total" fiber force acting across an area element in a possible diastolic configuration that lies in the θ = constant plane in the reference configuration and has area dA_θ in this configuration. The word "total" refers to the fact that we are taking into account the contribution of both fiber systems. Now

$$\underset{\sim}{d}F_\theta = \tfrac{1}{2}\rho\, dA_\theta T[(\underset{\sim}{n}_\theta \cdot \underset{\sim}{\tau}_+)\underset{\sim}{t}_+ + (\underset{\sim}{n}_\theta \cdot \underset{\sim}{\tau}_-)\underset{\sim}{t}_-], \tag{8}$$

with

$$\underset{\sim}{n}_\theta = (0, 1, 0), \tag{9}$$

$$\underset{\sim}{\tau}_{+,-} = \left(0, \frac{r}{(r^2 + B^2\lambda^2)^{1/2}}, \frac{\pm B\lambda}{(r^2 + B^2\lambda^2)^{1/2}}\right), \tag{10}$$

and

$$\underset{\sim}{t}_{+,-} = \left(0, \frac{R}{(R^2 + B^2)^{1/2}}, \frac{\pm B}{(R^2 + B^2)^{1/2}}\right). \tag{11}$$

By substitution, it follows that

$$\underset{\sim}{d}F_\theta = \rho \frac{R}{(R^2 + B^2)^{1/2}} \cdot \frac{r}{(r^2 + B^2\lambda^2)^{1/2}} \cdot T dA_\theta \underset{\sim}{i}_\theta. \tag{12a}$$

Let $\underset{\sim}{d}F_Z$ be the total fiber force acting across a material element in a possible diastolic configuration that lies in the Z = constant plane in the reference configuration and has area dA_Z in this configuration. By a similar approach, it can be shown that

$$\underset{\sim}{d}F_Z = \rho \frac{B^2}{(R^2 + B^2)^{1/2}} \cdot \frac{\lambda}{(r^2 + B^2\lambda^2)^{1/2}} \cdot T dA_Z \underset{\sim}{i}_Z. \tag{12b}$$

Note that in these formulas $\underset{\sim}{d}F_\theta$ *and* $\underset{\sim}{d}F_Z$ represent forces acting in an arbitrary end diastolic configuration, although they are proportional to the area of material elements lying in the coordinate surfaces of the reference configuration.

In mechanics any constraint, since it results in the prevention of some kinds of motion, must be maintained by forces. The incompressible nature of the myocardium represents one type of constraint, and it gives rise to a hydrostatic pressure field P within the heart wall. To maintain the constraint the pressure must be such that

$$\frac{\text{force}}{\text{unit volume}} = \nabla P \tag{13}$$

(Batchelor, 1970). We now derive a formula that describes how the pressure varies within the model heart wall and chamber.

Consider a thin cylindrical wedge of myocardium within the wall of the heart model in an arbitrary end diastolic configuration. Let the thickness of the wedge be dr and the height Δz. The angle the wedge subtends is 2Ψ. This wedge illustrated in Fig. 3.

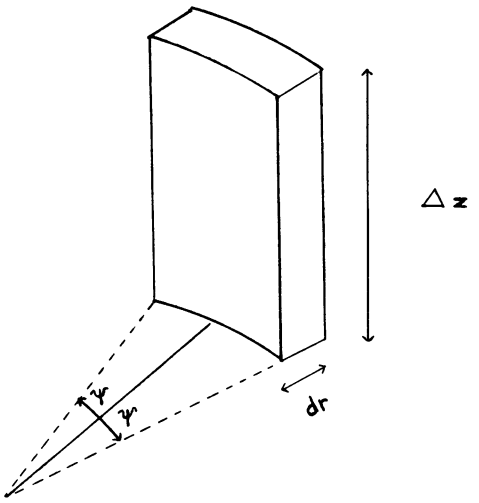

FIGURE 3 Schematic diagram of wedge volume element used in the derivation of the equation for local hydrostatic pressure in the wall. The volume element is an arbitrary diastolic configuration. Its height is Δz and its width is dr.

The net force acting across the two sides of the wedge due to the muscle fibers is

$$-2\,dF_\theta \sin \Psi \underset{\sim}{i}_r$$

or

$$-2\rho \frac{R}{(R^2 + B^2)^{1/2}} \cdot \frac{rT}{(r^2 + B^2\lambda^2)^{1/2}} \cdot \frac{dR\Delta z}{\lambda} \cdot \sin \Psi \underset{\sim}{i}_r.$$

The forces acting on the top of the wedge are equal in magnitude and opposite in direction to the forces acting on the bottom of the wedge, so that the contribution of these forces to the total force vanishes.

The volume of the wedge is $2\Psi r\,dr\,\Delta z$. Consequently, the total force per unit volume is

$$-\rho \frac{R}{(R^2 + B^2)^{1/2}} \cdot \frac{T}{\lambda(r^2 + B^2\lambda^2)^{1/2}} \cdot \frac{dR}{dr} \cdot \frac{\sin\Psi}{\Psi} \underset{\sim}{i}_r.$$

In the limit as $\Psi \to 0$, $\sin \Psi/\Psi = 1$.

Therefore

$$+\nabla P = \frac{\partial P}{\partial r} \underset{\sim}{i}_r, \text{ or} \tag{14}$$

$$\frac{\partial P}{\partial r} \underset{\sim}{i}_r = -\rho \frac{R}{(R^2 + B^2)^{1/2}} \cdot \frac{T}{\lambda(r^2 + B^2\lambda^2)^{1/2}} \cdot \frac{\partial R}{\partial r} \underset{\sim}{i}_r. \tag{15}$$

But $\dfrac{\partial P}{\partial r} = \dfrac{\partial P}{\partial R} \cdot \dfrac{\partial R}{\partial r}$, so that

$$\frac{\partial P}{\partial R} = -\rho \frac{R}{(R^2 + B^2)^{1/2}} \cdot \frac{T}{\lambda(r^2 + B^2\lambda^2)^{1/2}}, \tag{16}$$

$$P(R) = -\int_{R_i}^{R} \rho \frac{R}{\lambda(R^2 + B^2)^{1/2}} \cdot \frac{T}{(r^2 + B^2\lambda^2)^{1/2}} \, dR + P(R_i). \tag{17}$$

Here R_i is the radius of the inner (endocardial surface of the heart model. The pressure P still represents the hydrostatic pressure at r in the end diastolic configuration, but it has been referred back to R in the reference configuration, so that the domain of integration is fixed.

Applying the condition that the hydrostatic pressure at the outer (epicardial) surface of the heart vanishes, i.e., $P(R_o) = 0$, we obtain an equation for the filling pressure P_c:

$$P_c = P(R_i) = \int_{R_i}^{R_o} \rho \frac{R}{\lambda(R^2 + B^2)^{1/2}} \cdot \frac{T}{(r^2 + B^2\lambda^2)^{1/2}} \, dR. \tag{18}$$

The distribution of pressure across the wall of the heart model is

$$P(R) = \int_{R}^{R_o} \rho \frac{R}{\lambda(R^2 + B^2)^{1/2}} \cdot \frac{T}{(r^2 + B^2\lambda^2)^{1/2}} \, dR. \tag{19}$$

These equations for the pressure are applicable when the heart model is in a state of static equilibrium. We make the tacit assumption that end diastole corresponds to such a state. This assumption is reasonable because by the end of diastole the pressure is the same in both the left atrium and left ventricle for a period of time, referred to as the Z-point of the cardiac cycle by physiologists (Hurst and Logue, 1970).

The condition of static equilibrium implies that the net force acting on the free planar edge of the heart model is zero. Now two forces actually act across the plate; the hydrostatic pressure tends to push the plate down, while the muscle fibers pull the plate up. Net force balance thus requires that

$$\pi r_i^2 P_c + \int_{r_i}^{r_o} 2\pi r P(r) \, dr = \int_{r_i}^{r_o} dF_Z. \tag{20}$$

The left side of the above equation can be simplified by integrating by parts:

$$\int_{r_i}^{r_o} 2\pi r P(r) \, dr = -\pi r_i^2 P_c - \pi \int_{r_i}^{r_o} r^2 \frac{\partial P}{\partial r} dr. \tag{21}$$

Noting that $\partial P/\partial r = (\partial P/\partial R) \cdot (\partial R/\partial r)$ and $dr = (\partial r/\partial R)\, dR$, it follows that

$$\int_{r_i}^{r_o} r^2 \frac{\partial P}{\partial r} dr = \int_{R_i}^{R_o} r^2 \frac{\partial P}{\partial r} dR. \tag{22}$$

Substituting for $P(R)$, one obtains

$$\pi r_i^2 P_c + \int_{r_i}^{r_o} 2\pi r P(r) \, dr = \pi \int_{R_i}^{R_o} \rho \frac{r^2 R}{(R^2 + B^2)^{1/2}} \cdot \frac{T}{\lambda(r^2 + B^2\lambda^2)^{1/2}} \, dR. \tag{23}$$

On the other hand,

$$\int_{R_i}^{R_o} dF_Z = 2\pi \int_{R_i}^{R_o} \rho \frac{\lambda B^2 R}{(R^2 + B^2)^{1/2}} \cdot \frac{T}{(r^2 + B^2\lambda^2)^{1/2}} \, dR. \tag{24}$$

The condition for force equilibrium across the free end of the heart model is therefore

$$\int_{R_i}^{R_o} \rho \frac{R}{(R^2 + B^2)^{1/2}} \cdot \frac{T}{(r^2 + B^2\lambda^2)^{1/2}} \left(2\lambda B^2 - \frac{r^2}{\lambda}\right) dR = 0. \tag{25}$$

Choice of Reference Configuration and Muscle Fiber Properties

Up to now we have not specified the functional dependence of the muscle fiber force T nor stated explicitly any properties of the reference configuration. The forms of Eqs. 18 and 25 do not exclude the possibility of a diastolic configuration in which the simultaneous presence of fibers in states of compression (with $T < 0$) and extension (with $T > 0$) results in a net transmural pressure gradient, which we denote by ΔP, of zero. However, there is experimental evidence suggesting that fiber tension is in fact zero in all layers of the mammalian left ventricle when the difference in pressure between the inside and outside of the heart wall vanishes. In view of the importance of this point, this evidence is described in detail.

Spotnitz et al. (1966) have examined sarcomere length as a function of the filling pressure and volume under passive conditions in the intact left ventricles of dog and cat. Fresh hearts were excised from animals sacrificed acutely. The aorta and mitral orifices were sealed with clamps, and a cannula was inserted into the left main coronary artery. Two cannulas were inserted across the interventricular septum into the left ventricle: one to measure pressure, the other to introduce or withdraw fluid increments to regulate pressure. Fixation for electron microscopy followed adjustment of intraventricular conditions to a desired position on the pressure-volume curve. The preparation was perfused with fixative (glutaraldehyde) through the previously cannulated coronary artery. Previous studies have shown that this fixative does not change resting muscle tension (Sonnenblick et al., 1963). The sarcomere lengths from the inner, middle, and outer muscle layers were then measured by using electron microscopic techniques. Using this protocol, these investigators found that the sarcomere lengths in those preparations fixed in a state of zero transmural pressure gradient (i.e., with $\Delta P = 0$) ranged between 1.85 and 2.0 μm in the inner, middle, and outer layers of the heart wall. This fact is evident in figure 9 of their paper.

More recent experimental investigations of the resting sarcomere length-tension relation in isolated, microscopically thin ventricular muscle bundles have established that sarcomere lengths between 1.9 and 2.0 μm are associated with zero fiber tension. Kreuger and Pollack (1975) measured sarcomere lengths in thin, isolated rat papillary muscle using light diffraction techniques. Sarcomere length averaged 2.0 μm when diastolic fiber tension was zero. Pollack and Huntsman (1974) used bright field light microscopy and videometric techniques to determine the sarcomere length from the striation pattern in thin, live, right ventricular or papillary muscles of the rat. They found that minimal diastolic sarcomere length averaged between 1.9 and 2.0 μm; resting fiber tension was simultaneously measured in their preparations and found to be zero over this length range.

The evidence cited above suggests that a diastolic configuration corresponding to zero transmural pressure gradient and simultaneous zero fiber tension across the entire heart wall should be one of the possible configurations of a realistic model of the diastolic left ventricle. It is appropriate, then, to postulate a reference configuration in which $\Delta P = 0$, $T = 0$ for all fibers across the wall, and all fibers are assumed to have a sarcomere length of 1.9 μm in the reference state.

We emphasize that this reference configuration is adopted because of the above empirical data, not because it furnishes a trivial solution to Eq. 25 with $\Delta P = 0$.

Given this choice of reference configuration, the muscle fiber force T for $V > \overline{V}$ is not known in advance but constitutes part of the problem of determining the end diastolic configuration of the heart model. The length of a segment of a fiber in the reference configuration between $\theta = 0$ and $\theta = \theta'$ is $(R^2 + B^2)^{1/2} \cdot \theta'$. Similarly, the length of the same fiber segment in an arbitrary end diastolic configuration is $(r^2 + \lambda^2 B^2)^{1/2} \cdot \theta'$. The ratio of these two terms, which we denote by α, represents the degree of extension of a fiber in an arbitrary end diastolic configuration, relative to the reference configuration.

$$\alpha(R) = \left(\frac{r^2 + \lambda^2 B^2}{R^2 + B^2}\right)^{1/2}. \tag{26}$$

In the resting state, the tension-extension curve of heart muscle at lengths greater than its slack length is exponential in character (Braunwald, et al., 1976). It is appropriate, then, to let

$$T = D[e^{C(\alpha-1)} - 1], \tag{27a}$$

where D and C are constants, when $\alpha(R) \geq 1$. For $\alpha < 1$, the fibers resist compression and

$$T = -K(1 - \alpha). \tag{27b}$$

It is found when the anatomic distribution of fiber orientations is part of the model, α is always $\geqq 1$ across the heart wall in all possible end diastolic configurations.

Numerical Methods

Given the end diastolic volume V and with T specified by Eqs. 26 and 27, Eq. 25 represents a nonlinear equation for the unknown parameter λ. In this section we outline the numerical method used to determine λ. For this purpose, the fixed interval of integration (R_i, R_o) is divided into N segments of uniform length ΔR. The integral in Eq. 25 is replaced by the sum

$$F(\lambda) = \frac{5\Delta R}{288} \sum_{j=0}^{n-1} \sum_{k=0}^{5} \rho \epsilon_k \frac{R}{(R^2 + B^2)^{1/2}} \frac{T}{(r^2 + B^2\lambda^2)^{1/2}} \left(2\lambda B^2 - \frac{r^2}{\lambda}\right)$$

$$R = R_i + (5j + k)\Delta R \tag{28}$$

where $n = N/5$ and the ϵ_k represent the weighting coefficients in the fifth order Newton-Cotes closed integration formula:

$$\epsilon_0 = \epsilon_5 = 19; \epsilon_1 = \epsilon_4 = 75; \text{ and } \epsilon_2 = \epsilon_3 = 50.$$

Using the relations

$$\frac{dr^2}{d\lambda} = -\frac{1}{\lambda} r^2, \tag{29}$$

$$\frac{d\alpha}{d\lambda} = \frac{1}{2\alpha} \cdot \frac{(2\lambda^2 B^2 - r^2)}{\lambda(R^2 + B^2)}, \tag{30}$$

$$\frac{dT}{d\lambda} = DC\, e^{C(\alpha-1)} \cdot \frac{d\alpha}{d\lambda} \text{ for } \alpha \geq 1, \tag{31}$$

and

$$\frac{dT}{d\lambda} = K \cdot \frac{d\alpha}{d\lambda} \text{ for } \alpha < 1 \tag{32}$$

one can evaluate $dF/d\lambda$ explicitly. The equation $F(\lambda) = 0$ is solved by the iterative procedure

$$\lambda^{(m+1)} = \lambda^{(m)} - \frac{F'[\lambda^{(m)}]}{F[\lambda^{(m)}]} \tag{33}$$

(i.e., Newton's Method). In practice, this method converges efficiently, provided the initial estimate is sufficiently close to the actual root. To determine the range of possible end diastolic configurations, the chamber volume V is varied.

RESULTS

Choice of Model Parameters

To facilitate comparison with experimental data, the model parameters are chosen so that the model left ventricle has approximately the same dimensions and fiber structure as the canine left ventricle. Spotnitz et al. (1966) have found that zero filling pressure in the canine left ventricle requires a small initial volume of ~10 to 15 cc. Accordingly, we let $\overline{V}$, the chamber volume in the reference configuration, be 10 cc. The mass of the canine left ventricle is approximately 100 g, and the ratio of chamber length (i.e., major axis) to chamber diameter (i.e., minor axis) at end diastole is approximately 1.5 (Braunwald et al., 1976). If we require that the model satisfy these constraints, it is easily found that $R_i = 1.02$ cm, $R_o = 3.38$ cm, and $L = 3.06$ cm.

The distribution of fiber orientations in the canine left ventricle has been investigated by Streeter and co-workers (1969). They showed that the heart wall had a well-ordered distribution of fiber angles, and that this distribution of fiber angles did not vary appreciably at four representative sampling sites. To determine the function $B(R)$ in the model, the curve representing the mean of their data at these four sites, denoted by the points marked M in figure 4 of their paper, is digitized. $B(R)$ is then set equal to R times the absolute value of the tangent of the fiber angle. The fiber angle is always positive on account of the two symmetric fiber systems in the model ventricle. The distribution of fiber angles used to calculate $B(R)$ is shown in Fig. 2.

The muscle fiber parameters are $\rho D = 6.0$ g cm^{-2}, and $K = 10$ g cm^{-2}. The numerical parameters are as follows. The calculations are performed with the interval of integration (R_i, R_o) divided into 55 segments of uniform length ΔR. Sufficient iterations are carried out to reduce $|F(\lambda)|$ to less than 10^{-5} mm Hg at each diastolic volume.

Diastolic Pressure-Volume Relations

The relation between filling pressure and volume in the model ventricle is shown in Fig. 4. Zero filling pressure corresponds to the small initial volume of 10 cc. As the intraventricular volume increases, diastolic pressure rises, first slowly and then very rapidly. The model heart accommodates volume more by circumferential expansion than by axial extension. For example, with an increment of 40 cm^3 in intraventricular volume, r^2 changes by a factor of 3.42, while the length of the ventricle changes by a factor of 1.46.

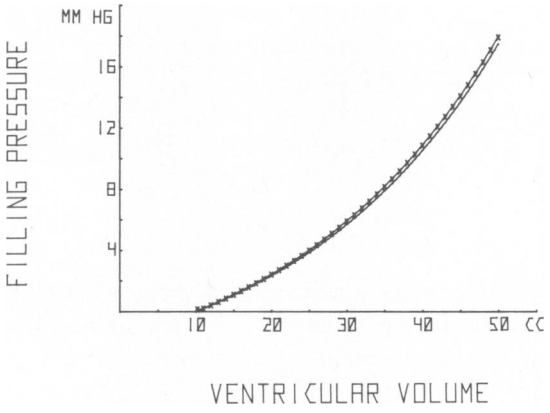

FIGURE 4 Relation between filling pressure and volume in the model ventricle (-x-x-). The plain line is a plot of the function $P = -a + be^{cV}$, with $a = 5.369$, $b = 3.738$, and $c = 0.0362$. Functions of this form have been found empirically to fit the diastolic pressure-volume relation of the canine left ventricle (see text).

Noble and associates (1969) have investigated diastolic pressure-volume relations in 7 conscious dogs. The left ventricular volume (V) was estimated by taking biplane cineradiographs with the left ventricular cavity previously outlined by permanent radiopaque markers. Left ventricular pressure (P) was measured with an implanted transducer. They found that the diastolic pressure-volume relationship was approximately exponential and was fitted by the equation $P = -a + b\,e^{cV}$, where a, b, and c are positive constants. The plain line in Fig. 4 is a plot of a function of this form with $a = 5.369$, $b = 3.738$, and $c = 0.0362$. There is close agreement between the pressure-volume curve of the model ventricle and this calculated function, suggesting that the model's behavior is representative of diastolic filling in vivo over a wide range of filling pressures.

Distribution of Pressure Across Heart Wall

The hydrostatic pressure field within the model heart wall at mechanical equilibrium, given by Eq. 19, is shown in Fig. 5. The 10 mm Hg chamber pressure in Fig. 5 A is in the normal physiological range, while the 21 mm Hg chamber pressure in Fig. 5 B is representative of the filling pressures encountered with acute pathological ventricular dilatation. Fig. 5 A demonstrates that the build up in hydrostatic pressure across the model heart wall, from zero on the epicardial surface to the left ventricular chamber pressure on the endocardial surface, departs strikingly from a simple linear relation. In the outer layers of the heart wall the pressure rises rapidly to a low value, compared with the chamber pressure. From 95 to 50% of wall thickness the rise in pressure is approximately linear, but the slope is minimal, so that a net gain of only 0.4 mm Hg is attained. At approximately 50% of wall thickness, the pressure-wall thickness curve has a point of inflection; the pressure then rises steeply in the subendocardial layers. The net gain in pressure occurring in the inner third of the heart wall is 85% of the left ventricular pressure.

A similar distribution of pressure across the model heart wall occurs at elevated filling pressures. This point is illustrated in Fig. 5 B. As the filling pressures increase, the absolute gradient in pressure between the subendocardium and the midwall also rises. For example,

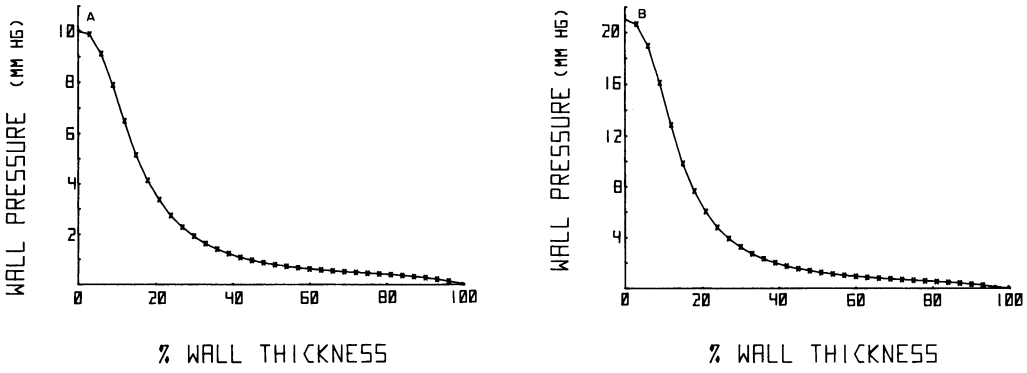

FIGURE 5 (A) Variation in hydrostatic pressure across the wall of the heart model when the chamber pressure is 10 mm Hg. (B) Variation in hydrostatic pressure across the wall of the heart model when the chamber pressure is 21 mm Hg.

this gradient is approximately 7.9 and 14.9 mm Hg at left ventricular filling pressures of 10 and 21 mm Hg, respectively.

Distribution of Fiber Force and Extension

The distribution of fiber extension within the model heart wall is plotted in Fig. 6 as a function of the left ventricular pressure. There is marked variation in the distribution of fiber extension; the fibers of the heart wall can be subdivided into three groups from a physiologic standpoint on the basis of their fiber extension-filling pressure curve.

The first group consists of fibers that are stretched beyond L_{max} even at the lower limit of normal physiologic filling pressures, i.e., 5 mm Hg. These fibers comprise the inner 30% of the heart wall. Their degree of extension-filling pressure curve is shown in Fig. 6 A. As the ventricular pressure increases, the degree of extension of these fibers continues to increase rapidly. For example, a fiber located at 10% of full wall thickness is stretched by 20, 34, and 43% at 5, 12, and 21 mm Hg, respectively. Since these fibers are always stretched beyond L_{max}, they cannot contribute to the operation of Starling's Law of Heart in the heart model.

The second group of fibers also does not contribute appreciably to the operation of Starling's Law of the Heart in the heart model. These fibers are located in the wall between 60–80% of wall thickness. Their degree of extension-filling pressure curve is shown in Fig. 6 A. As the ventricular pressure increases from 5 to 12 mm Hg, the degree of extension of these fibers hardly changes at all. For example, the degree of extension of a fiber located at 70% of full wall thickness changes by only 3.6% when the ventricular pressure is raised from 5 mm to 12 mm Hg. As the ventricular pressure increases to pressures above the normal physiologic ranges, the degree of extension of this group of fibers continues to increase with minimal slope.

The third group of fibers consists of those fibers that undergo appreciable extension below L_{max} as the ventricular pressure increases in the normal physiologic range. These fibers are located approximately 30–60% and 80–100% of full wall thickness. Their degree of extension-filling pressure curves is illustrated in Fig. 6 B. As the ventricular pressure approaches 12 mm Hg, the extension of the midwall fibers ranges from 13 to 15%. This degree

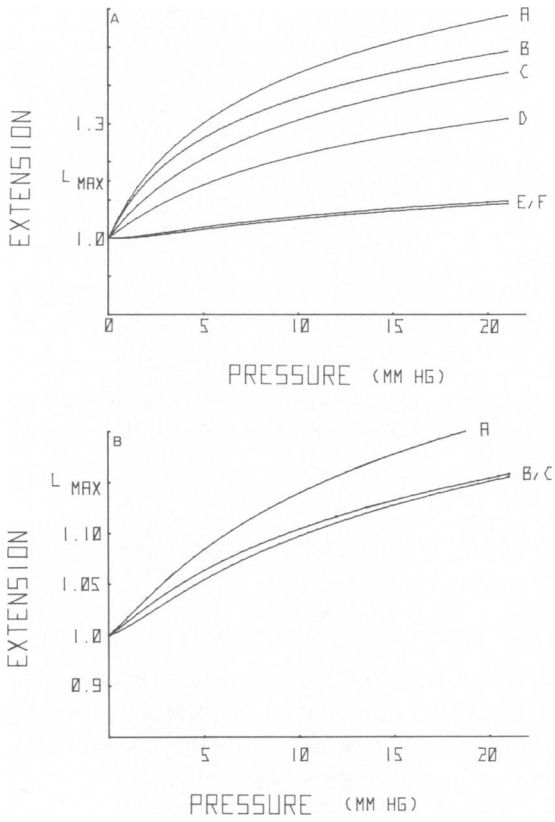

FIGURE 6 (A) Fiber extension at various representative locations within the model heart wall is plotted as a function of the filling pressure. The fibers corresponding to curves *A*, *B*, *C*, and *D*, located respectively at 9, 0, 20, and 29% of full wall thickness, do not contribute to the operation of Starling's Law of the Heart in the model, since they are stretched to L_{max} or beyond over the range of normal filling pressures (5–12 mm Hg). The fibers corresponding to curves *E* and *F*, located, respectively, at 80 and 69% of full wall thickness, do not stretch appreciably over the range of normal filling pressures. (B) Fiber extension at various representative locations within the model heart wall is plotted as a function of the filling pressure. The fibers corresponding to curves *A*, *B*, and *C* are located, respectively, at 40, 49, and 89% of full wall thickness. These fibers undergo appreciable extension below L_{max} as the ventricular pressure increases in the normal physiologic range.

of extension brings these fibers to the apex of the myocardial muscle cell length-tension curve. It is the third group of fibers that contributes to the operation of Starling's Law in the thick-walled heart model.

The distribution of fiber stress across the wall of the heart model at ventricular pressures of 10 and 21 mm Hg is shown in Fig. 7. The distribution of fiber stress mirrors the distribution of fiber extension; however, the peaks and valleys are accentuated because of the fibers' exponential length-tension relation. Note that maximal fiber force and extension occur in the subendocardial layers at approximately 7% of full wall thickness.

Figs. 6 and 7 suggest that the diastolic pressure-volume relation of the ventricle as a whole depends much more appreciably on the force balance achieved between fiber stress and hydrostatic pressure in the inner half than the outer half of the ventricular wall. To test this

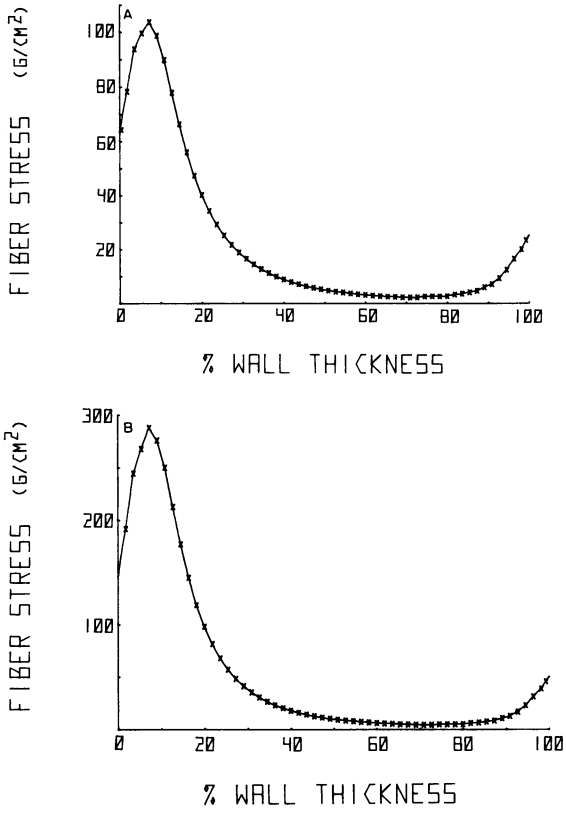

FIGURE 7 (A) The distribution of fiber stress across the wall of the heart model when the filling pressure is 10 mm Hg. (B) The distribution of fiber stress across the wall of the heart model when the filling pressure is 21 mm Hg.

idea, we divide the model heart into two cylinders, one representing the inner 50% of the heart wall and the second the outer 50% of the heart wall, and calculate the pressure-volume relation of each of these cylinders separately. Fig. 8 compares the pressure-change in volume relation of each of these "half heart" cylinders with the pressure-change in the volume relation of the whole heart model. Note that the cylinder representing the inner half of the heart model has almost the same pressure-volume relation as the total heart model, while the pressure-volume relation of the cylinder corresponding to the outer half of the heart wall is completely different. These results suggest that the diastolic pressure-volume relations of the heart depend primarily on the fiber architecture and forces in the inner half of the heart wall; the outer half of the heart wall is much more compliant and, for the most part, passively extended.

Effect of Heart Size

It is important to consider how the preceding results depend on the heart model's absolute size. The mammals are remarkable for their extraordinary range in size; the mammalian heart also varies in size over an extraordinary range. The heart of one of the smallest mammals, the dwarf bat (*Vesperugo pipistrellus*), weighs about 0.056 g, while the heart of

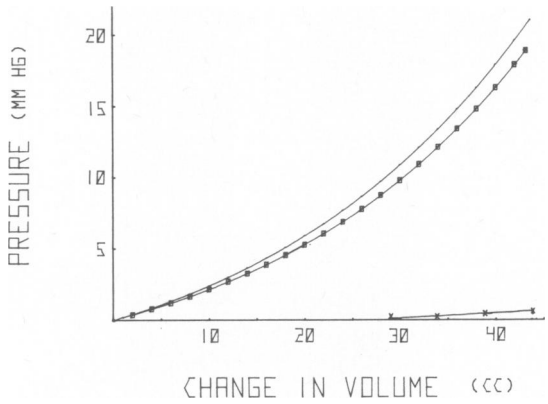

FIGURE 8 Pressure-change in volume relation of the whole heart model (----), inner half of heart model (-0-0-), and outer half of heart model (-x-x-).

the sperm whale weighs about 400,000 g (Clark, 1927). This represents a seven-million-fold variation in weight. Yet, the general shape and proportions of the heart remain quite similar over this wide range of size. For example, the heart of a rat magnified 25 Diam appears very similar to the heart of an ox (Clark, 1927). Clark (1927) has demonstrated that the weight of the heart in grams is approximately equal to the cube of the length in centimeters of the cavity of the left ventricle over a 30,000-fold range, from the 0.13 g heart of the mouse to the 3,900 g heart of the horse.

The foregoing considerations suggest that the hearts of mammals of different sizes are approximately scale models of each other. This provides the motivation for investigating the effect of heart size on the distribution of pressure and fiber extension across the wall in geometrically similar model hearts.

Specifically, let us consider two model hearts with proportional dimensions in their respective reference configurations: $R_i' = KR_i$, $R_o' = KR_o$, and $L' = KL$, where K is a constant. Given the same distribution of fiber angles in the two hearts, Eq. 2 implies that $B(R') = K\,B(R)$.

Suppose that the first heart chamber has volume $V' = K^3V$, while the second heart chamber has volume V. Let λ' and λ represent the axial extensions of the two heart models, relative to their reference configurations, in these respective states.

Now

$$r'^2 = \frac{1}{\lambda'}\left(R'^2 + \frac{V' - \bar{V}'}{\pi L'}\right) = K^2 r^2|_{\lambda=\lambda'}, \tag{34}$$

and

$$\alpha(R') = \alpha(R)|_{\lambda=\lambda'}. \tag{35}$$

The condition for force equilibrium for the first heart model is

$$\int_{R_i}^{R_o} \rho \frac{R'}{(R'^2 + B'^2)^{1/2}} \cdot \frac{T[\alpha(R')]}{(r'^2 + B'^2\lambda'^2)^{1/2}} \left(2\lambda' B'^2 - \frac{r'^2}{\lambda'}\right) dR' = 0. \tag{36}$$

or

$$K^2 \int_{R_i}^{R_o} \rho \frac{R}{(R^2 + B^2)^{1/2}} \cdot \frac{T[\alpha(R)]}{(r^2|_{\lambda=\lambda'} + B^2\lambda'^2)^{1/2}} \left(2\lambda' B^2 - \frac{r^2|_{\lambda=\lambda'}}{\lambda'}\right) dR = 0. \tag{37}$$

The latter equation is equivalent to the condition for force equilibrium for the second heart model, so that $\lambda' = \lambda$. It follows that $P_c' = P_c$ (Eq. 18) and $P(R') = P(R)$ (Eq. 19). For a family of heart models that are scale models of each other, the results of the preceding sections are thus independent of absolute heart size.

Effect of Fiber Architecture

The behavior of the heart model is, however, critically dependent on the existence of longitudinally oriented fibers in the endocardial and epicardial regions of the heart wall. To show this, we calculate the possible diastolic configurations of a second heart model in which the fiber orientation is circumferential across the entire wall. More specifically, in the second model, the anatomic distribution of fiber angles is altered so that the maximum fiber angle is 15° or less. This distribution of fiber angles is illustrated in Fig. 9.

Figs. 10, 11 and 12 demonstrate that when all the fibers are circumferential, the diastolic states of the model become completely different and, from a physiologic standpoint, untenable. The model heart now accommodates volume with a significantly greater degree of axial extension (Fig. 10). The diastolic pressure-volume relation is shifted so that the model heart is much more compliant at all chamber volumes (Fig. 11). Fig. 12 shows that as the filling pressure increases, the degree of fiber extension in a substantial portion of the middle heart wall remains less than one (i.e., these fibers undergo compression). This behavior is

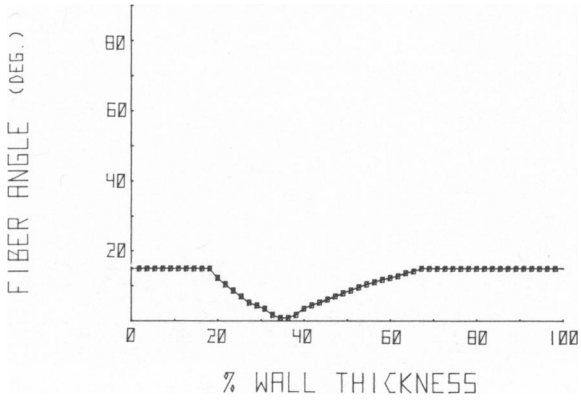

FIGURE 9 Modified distribution of fiber angles across model heart wall in which all fiber angles are 15° or less, so that all fibers pursue a predominantly circumferential course. This distribution of fiber angles is not anatomically correct.

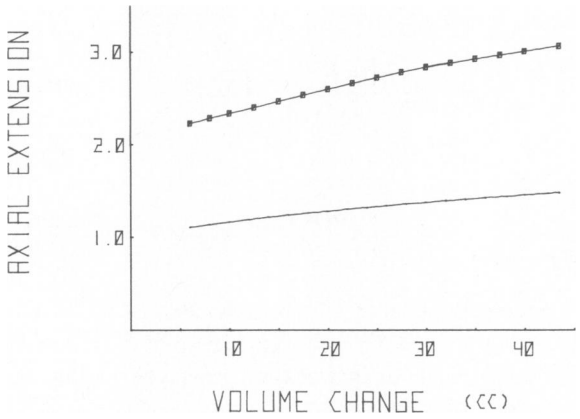

FIGURE 10 Axial extension of two heart models as a function of end diastolic volume change. The upper curve (-0-0-) corresponds to the heart model with only circumferential fibers (Fig. 9). The lower curve (—) corresponds to the anatomic distribution of fiber angles (Fig. 3).

unphysiologic because it makes the diastolic configurations of the model incompatible with effective systolic contraction.

With the results just described, it is assumed that fiber elements in the model resist extension but not compression, that $T = 0$ for $\alpha < 0$. There is however, experimental evidence that heart muscle fibers do in fact resist compression (Sonnenblick and Skelton, 1974). It is possible that the unphysiologic behavior of the heart model when all the fibers are circumferential results because this important feature of cardiac muscle physiology is omitted in the model.

To test this idea, we let the fibers resist compression as well as extension by setting

$$T = -K(1 - \alpha) \tag{38}$$

when $\alpha < 1$, where $K = 10$ g/cm^2, and recalculated the equilibrium configurations of the

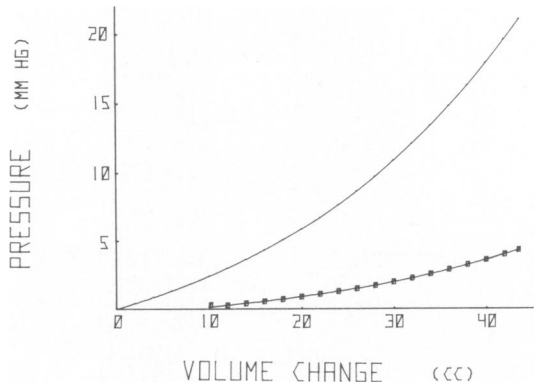

FIGURE 11 Pressure-volume change relation in two heart models. The upper curve (—) corresponds to the heart model with the anatomic distribution of fiber angles (Fig. 3). The lower curve (-0-0-) corresponds to the heart model with only circumferential fibers (Fig. 9).

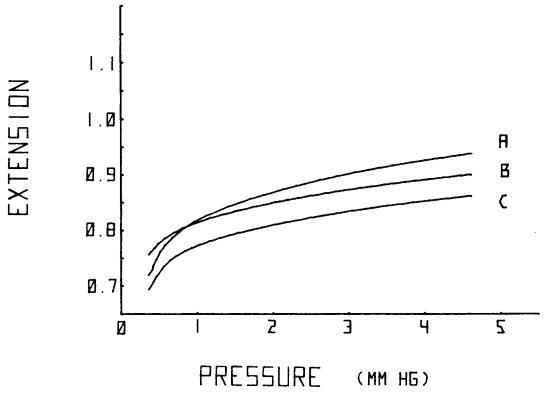

FIGURE 12 Fiber extension at representative locations as a function of filling pressure in the heart model with only circumferential fibers (Fig. 9). The fibers do not resist compression. Curves *A*, *B*, and *C* correspond, respectively, to 29, 49, and 40% of full wall thickness.

model. Fig. 13 demonstrates that in this case the degree of fiber extension in the middle heart wall still remains less than one.

DISCUSSION

Comparison with Experimental Data

Experimental determination of the distribution of myocardial fiber extension across the heart wall in vivo is not technically feasible at this time. The combined use of small implanted radio-opaque markers and fast computerized tomographic scanning may make such measurements possible in the near future. However, the myocardial cell sarcomere length is measurable, and the distribution of sarcomere length across the heart wall has been studied in

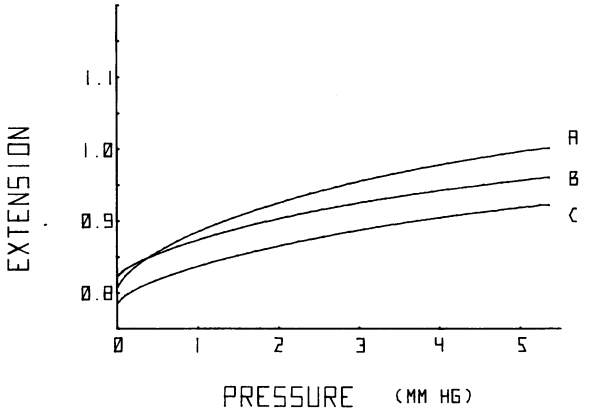

FIGURE 13 Fiber extension at representative locations as a function of filling pressure in the heart model with only circumferential fibers (Fig. 8). The fibers resist compression as well as extension (see text). Curves *A*, *B*, and *C* correspond, respectively, to 29, 49, and 40% of full wall thickness.

canine left ventricles that were fixed in situ in the open-chest dog during diastole by rapid, timed infusion of glutaraldehyde into the coronary arteries.

There is experimental evidence that the minimal resting cardiac sarcomere length is 1.9 μm (Grimm et al., 1970), sarcomere length is linearly related to fiber extension in the range of 1.9 to 2.2 μm, (Grimm et al, 1970; Pollack and Huntsman, 1974), and that sarcomere length ranges between 2.2 and 2.3 μm for large extensions (Sonnenblick et al, 1973). Given these data, it is appropriate to assign the fibers of the heart model a uniform sarcomere length of 1.9 μm in the reference configuration. We define the sarcomere length of a fiber in the model as 1.9 μm times the extension of the fiber, relative to its length in the reference configuration, up to an extension of 15.8% (equivalent to 2.2 μm).

The relation between diastolic sarcomere length and filling pressure in the intact ejecting heart has been investigated by Ross and co-workers (1967). Diastolic sarcomere lengths in the midwall of the left ventricle averaged 2.07 μm with a range of 2.05 to 2.15 μm, when filling pressure ranged from 6 to 8 mm Hg (Sonnenblick et al, 1967). This compares favorably with the calculated average sarcomere length of 2.06 μm in the midwall (i.e., 40–60% of wall thickness) fibers of the heart model. As filling pressure rises in the canine left ventricle, average sarcomere length increases, and when it reaches about 2.2 μm, filling pressure has reached 12–15 mm Hg. In the model ventricle, the calculated average sarcomere length of midwall fibers is 2.15 and 2.19 μm at filling pressures of 12 and 15 mm Hg, respectively. In the subendocardial layers of the canine left ventricle, sarcomeres tend to be longer than in the outer layers (Diamond et al., 1971), and the longest sarcomeres are found between the subendocardial and midwall layers (Mitchell et al., 1960). The calculated distribution of sarcomere lengths in the model ventricle has the same qualitative features.

Diamond and co-workers (1971) have investigated the effect of heart size on sarcomere length. Despite a ten-fold difference in size of the heart, they found the relation between filling pressure and sarcomere length to be identical in the cat and dog. On the basis of these observations, they conclude that diastolic filling pressure, or wall tension, is the general determinant of diastolic sarcomere length in the normal left ventricle independent of the absolute size of the heart. As discussed in the preceding section, the relation between filling pressure and fiber extension in the heart model is also independent of absolute heart size for a family of heart models that are scale models of each other. Geometric similarity of mammalian hearts is an empirical fact.

A variety of methods, including the use of embedded arteries (Gregg and Eckstein, 1941; Johnson and Dipalma, 1939; Salisbury et al., 1962), pockets of fluid (Laszt and Muller, 1958), plastic tubing (Brandi and McGregor, 1969), latex balloons (Dieudonne, 1967; D'Silva et al., 1963), needles (Kirk and Honig, 1964), and embedded miniature pressure transducers (Armour and Randall, 1970) have been employed to measure intramyocardial pressure. However, the results of these studies are widely divergent, and there is lack of agreement on the actual variation in hydrostatic pressure across the heart wall. This variability may result because any implanted measuring device probably, in itself, alters the local fiber structure and tension, and thereby perturbs the intramyocardial pressure. It is thus not possible to compare the variation in pressure across the wall of the heart model with well validated experimental data at this time.

Physiologic Significance of Results

The numerical calculations suggest that the functional role of heart muscle fiber depends quite significantly on its relative position in the heart wall. For example, the mechanical equilibrium corresponding to end diastole in the heart model depends disproportionately on the fibers of the inner half of the heart wall. While our results provide support for the view that Starling's Law of the Heart is in part a reflection of the fact that changes in end diastole volume alter the degree of myocardial fiber extension, the computations also show that only approximately 50% of the fibers in the model heart wall can contribute to the Frank-Starling mechanism. The fibers of the subendocardium are stretched beyond L_{max} at low filling pressures, while the circumferentially oriented fibers between 60–80% of full wall thickness stretch with minimal slope as the ventricular volume increases. The latter finding may seem surprising in view of the fact that the model heart accommodates intraventricular volume by circumferential expansion. The apparent explanation for this finding is that the thinning of the heart wall that occurs with increasing intraventricular volume (a consequence of the myocardium's incompressibility) substantially reduces the actual radial displacement of these fibers in 3-space.

The subendocardial fibers operate in a "mechanical milieu" distinctly different from the other model heart wall muscle fibers. In diastole they are stretched beyond L_{max} and have a high resting tension. Conversely, during systolic ejection they must shorten far more than the rest of the myocardial fibers. In view of the inverse relation between muscle force and velocity in cardiac muscle, these fibers develop less active tension than the rest of the fibers in the heart wall. During diastole, the hydrostatic pressure in the subendocardial layers of the heart wall is significantly greater than in the rest of the myocardium. These findings are of special interest because perfusion of the subendocardium, unlike the rest of the heart wall, takes place primarily during diastole (Domenech et al., 1969; Downey and Kirk, 1974). The model calculations predict that elevation of left ventricular end diastole pressure increases the absolute pressure gradient between the subendocardium and the midwall and outer layers of the heart wall. It is possible that in a compromised coronary vascular bed this pressure gradient could stop perfusion of the subendocardium and initiate infarction. The subendocardial region of the left ventricular wall is known to be the region of the heart wall in greatest jeopardy in coronary artery disease (Griggs and Nakamura, 1968) and most vulnerable to ischemia (Horn et al., 1950; Braunwald et al., 1976).

The results suggest that the diastolic properties of the left ventricle are strongly dependent on the heart wall's fiber architecture. The marked variation in the distribution of fiber force across the wall at end diastole is a consequence of the anatomic distribution of fiber orientations. The diastolic compliance of the model is substantially increased when all the fibers of the model pursue a predominantly circumferential helical course. While previous model work on the diastolic left ventricle has taken into account nonnegligible wall thickness, incompressibility, finite deformation, and nonlinear elastic effects, the fiber architecture of the ventricular wall is largely ignored in theoretical formulations of cardiac mechanics. For example, the investigations of Janz and co-workers (Janz and Grimm, 1973; Janz et al., 1974; Janz and Waldron, 1978) and Mirsky and associates (Mirsky, 1969; Mirsky et al., 1974) treat the ventricle as an isotropic, thick-walled solid of revolution.

Streeter and associates (Streeter and Basset, 1966; Streeter, 1969; Streeter et al., 1970) use a model for ventricular stress analysis that incorporates varying fiber orientation; however, to calculate wall forces, a constant tension is assumed for each fiber through the wall. Janz and Waldron (1976) derive a model for myocardial nonhomogeneity based on the assumption that circumferential fiber stress is independent of position in the ventricular wall. Glantz and Kernoff (1975) calculate the muscle stiffness from canine left ventricular pressure-volume curves using a model based on a similar assumption. The numerical computations presented here imply that a realistic formulation of diastolic ventricular mechanics must take into account possible variation in fiber force across the heart wall, as well as its fiber architecture.

SUMMARY AND CONCLUSIONS

In the present paper we have formulated a model for diastolic ventricular mechanics that takes into account nonnegligible wall thickness, incompressibility, finite deformation, nonlinear elastic effects, and the known fiber architecture of the ventricular wall. Twisting motion during diastolic filling is avoided in the model by dividing the anatomic distribution of fiber orientations into a clockwise and counterclockwise system. In the reference configuration, there is no net difference in pressure between the inner and outer walls, the fiber force is assumed to be zero across the wall, and all fibers are assigned a sarcomere length of 1.9 μm. Wall forces and the geometrical configuration of the heart at end diastole are interdependent.

Numerical evaluation of the possible end diastolic configurations of the model allows one to make detailed predictions about the mechanical state of the left ventricle at end diastole. The distribution of fiber extension across the wall is found to be highly variable. Subendocardial fibers are stretched beyond L_{max} even at low filling pressures, i.e., 5 mm Hg. Fibers located between 60–80% of wall thickness extend minimally between 5–12 mm Hg. Only about 50% of the wall's muscle fibers contribute to the operation of the Frank-Starling mechanism. The hydrostatic pressure field within the wall is highly nonlinear. The pressure rises steeply in the subendocardial layers so that the net gain in pressure in the inner third of the wall is 85% of the filling pressure. With pathologically elevated filling pressures, the absolute pressure gradient between the subendocardium and the midwall increases proportionately. In the model the inner half of the heart wall plays disproportionately greater role than the outer half in determining diastolic compliance. These predictions should be helpful in planning experiments designed to increase our understanding of ventricular function in diastole.

The author gratefully acknowledges the encouragement and support of Dr. Charles S. Peskin of the Courant Institute of Mathematical Sciences (NYU), Dr. Jacob Lubliner of the Department of Civil Engineering, University of California, Berkeley, Dr. Ralph Cavalieri, and Dr. David Bristow of the Department of Medicine, University of California, San Francisco. The author is also indebted to Mrs. Rita Lieu for her gracious kindness, excellent typing, and editorial assistance.

This work was supported in part by the National Institutes of Health (Public Health Service grant 5T5Gm1674).

Received for publication 28 June 1978 and in revised form 22 June 1979.

REFERENCES

ARMOUR, J. A., and W. C. RANDALL. 1971. Canine left ventricular intramyocardial pressures. *Am. J. Physiol.* **220**:1833.

BATCHELOR, G. H. 1970. An Introduction to Fluid Mechanics. Cambridge University Press, London. 15.
BRANDI, G., and M. MCGREGOR. 1969. Intramural pressure in the left ventricle of the dog. *Cardiovasc. Res.* **3**:472.
BRAUNWALD, E., J. ROSS, and E. H. SONNENBLICK. 1976. Mechanisms of Contraction of the Normal and Failing Heart. Little, Brown and Company, Boston. 72.
CLARK, A. J. 1927. Comparative Physiology of the Heart. Macmillan Company, New York. 87.
DIAMOND, G., J. S. FORRESTER, J. HARGIS, W. W. PARMLEY, R. DANZIG, and H. J. C. SWAB. 1971. The diastolic pressure-volume relationship of the canine left ventricle. *Circ. Res.* **29**:267.
DIEUDONNE, J. M. 1967. Tissue-cavitary difference pressure of dog myocardium under stress. *Am. J. Physiol.* **213**:107.
DOMENECH, R. J., J. I. E. HOFFMAN, M. I. M. NOBLE, K. B. SAUNDERS, J. R. HENSON, and S. SUBIJANTO. 1969. Total and regional coronary blood flow measured by radioactive microspheres in conscious and anesthetized dogs. *Circ. Res.* **25**:581.
DOWNEY, J. M., and E. S. KIRK. 1974. Distribution of the coronary blood flow across the canine heart wall during systole. *Circ. Res.* **34**:251.
D'SILVA, J. L., D. MENDEL, and M. C. WENTERTON. 1963. Effect of sympathetic amines on intramyocardial pressure in the rabbit. *Am. J. Physiol.* **205**:10.
GLANTZ, S. A., and R. S. KERNOFF. 1975. Muscle stiffness determined from canine left ventricular pressure-volume curves. *Circ. Res.* **37**:787.
GREGG, D. E., and R. W. ECKSTEIN. 1941. Measurements of intramyocardial pressure. *Am. J. Physiol.* **132**:781.
GRIGGS, D. M., JR., and Y. NAKAMURA. 1968. Effect of coronary constriction on myocardial distribution of iodoantipyrine-131-I. *Am. J. Physiol.* **215**:1082.
GRIMM, A. F., K. V. KATELE, R. KUBOTA, and W. V. WHITEHORN. 1970. Relation of sarcomere length and muscle length in resting myocardium. *Am. J. Physiol.* **218**:1412.
HORN, H., L. E. FIELD, S. DACK, and A. M. MASTER. 1950. Acute coronary insufficiency: pathological and physiological aspects. Analysis of twenty-five cases of subendocardial necrosis. *Am. Heart J.* **40**:63.
HURST, J. W., and I. LOGUE. 1970. The Heart, Arteries and Veins. McGraw-Hill Book Company, New York. 76.
JANZ, R. F., and A. F. GRIMM. 1973. Deformation of the diastolic left ventricle. I. Nonlinear elastic effects. *Biophys. J.* **13**:689.
JANZ, R. F., and R. J. WALDRON. 1978. Predicted effect of chronic apical aneurysms on the passive stiffness of the human left ventricle. *Circ. Res.* **42**:255.
JANZ, R. F., B. R. JUBERT, and T. F. MORIARTY. 1974. Deformation of the diastolic left ventricle. II. Nonlinear geometric effects. *J. Biomech.* **7**:509.
JOHNSON, J. R., and J. R. DI PALMA. 1939. Intramyocardial pressure and its relation to aortic blood pressure. *Am. J. Physiol.* **125**:234.
KIRK, E. S., and C. R. HONIG. 1964. An experimental and theoretical analysis of myocardial tissue pressure. *Am. J. Physiol.* **207**:361.
KREUGER, J. W., and G. H. POLLACK. 1975. Myocardial sarcomere dynamics during isometric contraction. *J. Physiol. (Lond.).* **251**:627.
LASZT, V. L., and A. MULLER. 1958. Der Myocardiale Druck. *Helv. Physiol. Pharmacol. Acta.* **16**:88.
MIRSKY, I. 1969. Left ventricular stresses in the intact human heart. *Biophys. J.* **9**:189.
MIRSKY, I., D. N. GHISTA, and H. SANDLER. 1974. Cardiac Mechanics: Physiological, Clinical and Mathematical Considerations. John Wiley & Sons, Inc., New York. 45.
MITCHELL, J. H., R. J. LINDEN, and S. J. SARNOFF. 1960. Influence of cardiac sympathetic and vagal nerve stimulation on the relation between left ventricular diastolic pressure and myocardial segment length. *Circ. Res.* **8**:1100.
NOBLE, M. I. M., E. N. C. MILNE, R. J. GOERKE, E. CARLSSON, R. J. DOMENECH, K. B. SAUNDERS, and J. I. E. HOFFMAN. 1969. Left ventricular filling and diastolic pressure-volume relations in conscious dogs. *Circ. Res.* **24**:269.
PATTERSON, S. W., and E. H. STARLING. 1914. On mechanical factors which determine output of ventricles. *J. Physiol. (Lond.).* **48**:357.
POLLACK, G. H., and L. L. HUNTSMAN. 1974. Sarcomere length-active force relations in living mammalian heart muscle. *Am. J. Physiol.* **227**:383.
ROSS, J. JR., E. H. SONNENBLICK, J. W. COVELL, G. A. KAISER, and D. SPIRO. 1967. Architecture of the heart in systole and diastole: technique of rapid fixation and analysis of left ventricular geometry. *Circ. Res.* **21**:409.
SALISBURY, P. F., C. E. CROSS, and P. A. RIEBEN. 1962. Intramyocardial pressure and strength of left ventricular contraction. *Circ. Res.* **10**:608.

SONNENBLICK, E. H., and C. L. SKELTON. 1974. Reconsideration of the ultrastructural basis of cardiac length-tension relations. *Circ. Res.* **35**:517.

SONNENBLICK, E. H., D. SPIRO, and J. S. COLTRELL. 1963. Fine structural changes in heart muscle in relation to the length-tension curve. *Proc. Natl. Acad. Sci. U.S.A.* **49**:193.

SONNENBLICK, E. H., C. L. SKELTON, W. D. SPOTNITIZ, and D. FELDMAN. 1973. Redefinition of the ultrastructural basis of cardiac length-tension relations. *Circulation.* **48**:65 (Suppl. 4).

SONNENBLICK, E. H., J. ROSS, JR., J. W. COVELL, H. M. SPOTNITIZ, and D. SPIRO. 1967. The ultrastructure of the heart in systole and diastole. *Circ. Res.* **21**:423.

SPOTNITZ, H. M., E. H. SONNENBLICK, and D. SPIRO. 1966. Relation of ultrastructure to function in the intact heart: Sarcomere structure relative to pressure volume curves of the intact left ventricles of dog and cat. *Circ. Res.* **18**:49.

STREETER, D. D., JR. 1969. A rational model for myocardial stress analysis based on fiber orientation and curvature. Ph.D. Thesis. The Catholic University of America, Washington.

STREETER, D. D., JR., and D. L. BASSETT. 1966. An engineering analysis of myocardial fiber orientation in pig's left ventricle in systole. *Anat. Rec.* **155**:503.

STREETER, D. D., JR., W. E. POWERS, M. A. ROSS, and F. TORRENT-GUASP. 1978. Three-dimensional fiber orientation in the mammalian left ventricular wall. In: Cardiovascular System Dynamics. J. Baan et al., editors. M.I.T. Press, Cambridge. 73.

STREETER, D. D., JR., H. M. SPOTNITZ, D. P. PATEL, J. ROSS, JR., and E. H. SONNENBLICK. 1969. Fiber orientation in the canine left ventricle during diastole and systole. *Circ. Res.* **24**:339.

STREETER, D. D., JR., R. N. RAMESH, D. J. PATEL, H. M. SPOTNITZ, J. ROSS, JR., and E. H. SONNENBLICK. 1970. Stress distribution in the canine left ventricle during diastole and systole. *Biophys. J.* **10**:345.